HHS Public Access

Author manuscript

ACS Sens. Author manuscript; available in PMC 2023 March 08.

Published in final edited form as:

ACS Sens. 2023 January 27; 8(1): 19–27. doi:10.1021/acssensors.2c01341.

GPCR signaling measurement and drug profiling with an automated live-cell microscopy system

Eric Greenwald[1], **Clara Posner**[2], **Ananya Bharath**[3], **Anne Lyons**[2], **Cristina Salmerón**[1], **Krishna Sriram**[1], **Shu Z. Wiley**[1], **Paul A. Insel**[1,4,*], **Jin Zhang**[1,2,5,*]

[1]Department of Pharmacology, University of California, San Diego, La Jolla, CA 92093, USA

[2]Department of Bioengineering, University of California, San Diego, La Jolla, CA 92093, USA

[3]Department of Chemical Engineering, University of California, San Diego, La Jolla, CA 92093, USA

[4]Department of Medicine, University of California, San Diego, La Jolla, CA 92093 USA

[5]Department of Chemistry and Biochemistry, University of California, San Diego, La Jolla, CA 92093, USA

Abstract

A major limitation of time-lapse microscopy combined with fluorescent biosensors, a powerful tool for quantifying spatiotemporal dynamics of signaling in single living cells, is low experimental throughput. To overcome this limitation, we created a highly customizable, MATLAB-based platform: FALCOscope (Flexible Automated Liquid-handling Combined Microscope) that coordinates an OpenTrons liquid handler and a fluorescent microscope to automate drug treatments, fluorescence imaging and single cell analysis. To test the feasibility of the FALCOscope, we quantified G protein-coupled receptor (GPCR)-stimulated Protein Kinase A (PKA) activity and cAMP responses to GPCR agonists and antagonists. We also characterized cAMP dynamics induced by GPR68/OGR1, a proton-sensing GPCR, in response to variable extracellular pH's. GPR68-induced cAMP responses were more transient in acidic than neutral pH's, suggesting a pH-dependence for signal attenuation. Ogerin, a GPR68 positive allosteric modulator, enhanced cAMP response most strongly at pH 7.0 and sustained cAMP response for acidic pH's, thereby demonstrating the capability of the FALCOscope to capture allosteric modulation. At a high concentration, ogerin increased cAMP signaling independent of GPR68, likely via phosphodiesterase inhibition. The FALCOscope system thus enables

*To whom correspondence and material requests should be addressed (pinsel@health.ucsd.edu, jzhang32@health.ucsd.edu).

AUTHOR CONTRIBUTIONS

E.C.G. and J.Z. conceived the project. E.C.G., C.P., C.S., P.A.I. and J.Z. designed all experiments. E.C.G. built the FALCOscope, developed cell segmentation scripts and performed the AKAR4 dose screening, antagonist/agonist screening experiments. C.S., S.W. and K.S. developed and validated the GPR68 OE HEK293 cell line; C.S. performed qPCR and immunohistochemistry verification. C.P. and A.B. performed the pH change and ogerin experiments. C.P., A.B., and A.L. performed ogerin off-target effect imaging experiments. C.S. performed the PDE activity assay. E.C.G., C.P., P.A.I. and J.Z. wrote the manuscript; all authors gave feed-back on the manuscript.

SUPPORTING INFORMATION.

Supporting Information Available: The following files are available free of charge. Additional methods and experimental details and supporting experimental results and analysis (DOC).

COMPETING INTERESTS

The authors declare no competing interests.

enhanced throughput single-cell dynamic measurements and is a versatile system for interrogating spatiotemporal regulation of signaling molecules in living cells and for drug profiling and screening.

Graphical Abstract

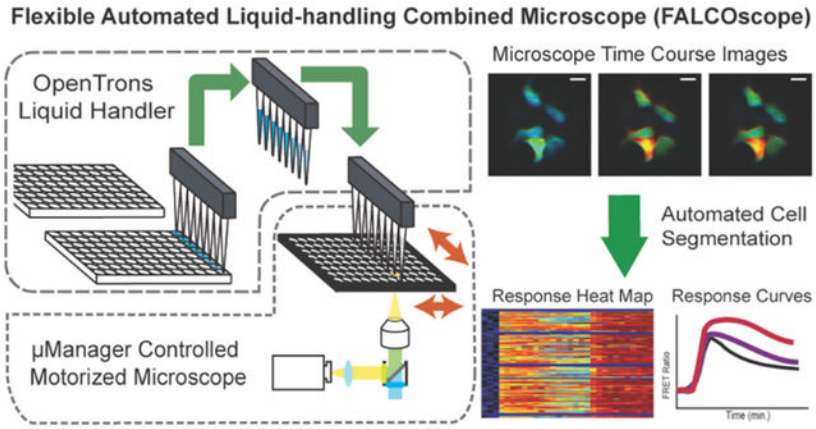

Keywords

genetically encoded biosensor; fluorescence imaging; FRET; signaling; GPCR; cAMP; high content

G protein-coupled receptors (GPCRs) are an important class of signaling molecules and drug targets[1]. More than 100 GPCRs are termed orphan receptors, i.e. without physiological agonists[2,3]. Additionally, complex, multimodal GPCR activation and downstream signaling is an area of active investigation[4]. Functional assays that assess receptor activation and downstream signaling are widely used in GPCR biology and drug discovery[5,6]. For GPCRs that lack structural information[7], high-throughput screening of compounds and peptides in functional assays is widely used in drug discovery[5]. Genetically encoded fluorescent biosensors have enabled live-cell assays for evaluating GPCR responses[8]. Such biosensors for cAMP and Protein Kinase A (PKA) activity are widely used in functional characterization of $G\alpha_s$-coupled GPCRs, which stimulate the trimeric GTP binding protein G_s. G_s activates adenylyl cyclase (AC), increasing cAMP production, and cAMP in turn activates PKA.

Fluorescent biosensors are useful tools to assess live cell signaling in microplate reading or microscopy formats. While extraction-based biochemical assays (e.g., immunoassays, immunoblotting) typically provide data on several minute time-scales, fluorescent biosensor-based assays can achieve nondestructive continuous measurements on a second or even millisecond timescale[8]. Moreover, imaging enables the detection of signaling activity in individual cells[8,9], thereby facilitating detection of responses of cellular sub-populations, spatiotemporal dynamics, such as asynchronous oscillations, that may be obscured by heterogeneity, and subcellular differences of signaling activities[10,11].

Even so, the throughput of microscopy is typically low, especially when drug additions are manually applied during time-lapse experiments. To overcome this limitation, we built a Flexible Automated Liquid-handling Combined Microscope (FALCOscope) system that leverages a programmable open-source liquid handler for automated drug stimulations during time-lapse imaging experiments. The FALCOscope automates single-cell imaging experiments with multiple drug stimulations on 96-well plates. Here, we show the capabilities of the FALCOscope in three different contexts: drug concentration screening, drug response profiling, and characterization, including interaction with an allosteric activator, of GPR68/OGR1, a pH-sensing GPCR. These studies reveal unexpected impact of both orthosteric and allosteric agonists on the kinetics of functional responses.

METHODS

FALCOscope Development.

An automated fluorescent microscope compatible with the μManager software (https://micro-manager.org/) was selected. The Zeiss AxioObserver Z1 (Carl Zeiss inc) microscope contains a motorized filter cube, objective wheels, automated excitation and emission focus wheels, hardware autofocus (Zeiss Definite Focus), an automated motorized stage (Prior Scientific), and a CMOS Orca Flash 4.0 camera (Hamamatsu). The bright field lamp was excluded to enable placement of the Opentrons OT1 (Opentrons Inc) liquid handler above the microscope stage. We mounted an Opentrons OT1 above the microscope stage by connecting T slot aluminum rails to the bottom of the OT1 and to the CleanBench air table (TMC Vibration Control/AMETEK). A section of the OT1 base plate was cut out to enable access of the liquid handling pipettes to the microscope stage sample area. A bespoke acrylic incubation enclosure with an IncuKit temperature control system (Incubator Warehouse) and 5% CO2 supply was built around both the microscope base and OT1 liquid handler to maintain cells at 37°C during experiments.

FALCOscope software was created in MATLAB 2017a (Math-works inc) by utilizing a previously developed MATLAB to μManager API and direct MATLAB to Python function calls to the OT Python API. A MATLAB library was developed to define and execute a queued list of image acquisition and liquid handling operations.

Cell culture and Imaging Preparation.

HEK293T, HEK293, and HEK293 GPR68OE cells were maintained in Dulbecco's modified Eagle medium (DMEM; Gibco 11885–084) supplemented with 10% FBS (FBS; Gibco 26140–079) and 1% (v/v) penicillin and streptomycin (Pen/Strep; Gibco 15140–122) with 4.5 g/L glucose at 37°C and with 5% CO2. 96 well glass bottom plates (Cellvis, #P96–1.5H-N) were coated with 100 μg/mL Poly-D-Lysine (Sigma, P0899–100MG) in sterile Dulbecco's Phosphate Buffered Saline (DPBS (1X); Gibco 14190–144) for 1h at 37°C and washed twice with sterile DPBS before HEK293T cells were plated. 24h after plating, cells were transfected using PolyJet (SignaGen) and 100 ng of either the AKAR4 biosensor (Addgene, 61619) or the EpacS-H188 biosensor (Addgene, 170349) per well. 12–24 h after transfection, cells were prepared for imaging by incubating with 1 μM Hoescht 33342 (Cell Signaling, 4082S) for 20–30 min, washed once with DPBS. Cells were then incubated

in 200 μL of Hanks balanced salt solution (HBSS, Gibco 14065–056) buffered with 20 mM HEPES, pH 7.4 and supplemented with 2 g/L glucose for at least 30 min at 37°C prior to imaging. For pH change experiments, 250 μL of HBSS media at pH 8.5 was added to each well instead. Before imaging, the imaging plate was sealed using X-Pierce, a sterile pierceable vinyl plate sealing film (Genesee Scientific), to prevent contamination and evaporation of buffer during imaging experiments.

FALCOscope Experiments.

Time-lapse epifluorescence images were ac. quired with a plan-apochromat 10x/0.45 NA objective (Carl Zeiss) in the dark at 37°C. CFP was imaged with an ET420/30x excitation filter, ET470/40m emission filter, and T455lpxt dichroic. YFP was imaged with an ET495/10x excitation filter, ET535/25m emission filter, and T5151p dichroic. CY FRET was imaged with an ET420/30x excitation filter, ET535/25m emission filter, and T5151p dichroic. DAPI was imaged with an ET380x excitation filter, ET470/40m emission filter, and T455lpxt dichroic.

Using single column batches across a 96 well plate, we acquired images in 1-min intervals. For drug additions, 100μL of imaging media was aspirated from the column on the imaging plate and then mixed into the drug plate by the OT1 using an 8-channel pipette. Compounds were delivered simultaneously to the 8 wells in the column being imaged and mixed three times. pH media exchange was performed by aspirating 200 μL HBSS from the imaging plate and discarding in a waste plate, adding 200 μL of fresh pH HBSS to the imaging plate, and mixing gently 3 times. This pH exchange was performed three times.

At the end of each experiment, cells were treated with the adenylyl cyclase activator forskolin (Fsk; 50 μM) and the phosphodiesterase inhibitor IBMX (100 μM) to elicit a maximal biosensor response for data normalization and quality control. After single responses were quantified, cells with a maximum Fsk/IBMX response between 1.5 to 4 times the baseline emission ratio were chosen for further analysis.

Statistical Analysis.

Ordinary one-way ANOVA with Dunnett’s test for multiple comparisons was performed using GraphPad Prism 9 (GraphPad Software) for all comparisons except for the fluorescein pH test (Supplementary Figure 4) and the area under the curve comparisons (Supplementary Figure 10 and 11). The fluorescein pH test and area under the curve comparisons were performed using an unpaired, one-tailed t-test in GraphPad Prism 9. Statistical significance was set at $p < 0.05$ with a 95% confidence interval. Averaged live-cell imaging time courses depict mean ± 95% confidence interval. Scatter plot bar graphs depict the mean ± standard error of the mean. Violin plots depict the median (dashed line) and the quartiles (dotted lines).

RESULTS AND DISCUSSION

Development of the FALCOscope.

To automate and increase the throughput of live-cell fluorescent biosensor imaging experiments, we developed the FALCOscope. We expanded on μManager[12], an existing open-source software for automated time-course imaging, by combining it with a liquid handling robot for automated drug delivery. The FALCOscope coordinates three tasks in MATLAB: 1) interfacing with the microscope to enable higher throughput time-lapse imaging; 2) controlling an open-source liquid handler; and 3) analyzing images and storing data (Figure 1).

The FALCOscope system utilizes the application program interface (API) for μManager within MATLAB to operate components of a motorized microscope (Supplementary Figure 1). This integration leverages μManager's optimized graphical user interface to execute microscope-specific functions, e.g., acquiring images and changing filter sets. To enable image collection across a multi-well plate, we incorporated the specification of the size and spacing of the wells of a 96-well plate into μManager's multi-position image acquisition settings. The FALCOscope also records metadata for each image, such as microscope configuration, acquisition time, well or position in a well, and experimental conditions of that well.

We used the liquid handler OT1 (OpenTrons) to automate the delivery of drugs and stimuli since its open-source software could be integrated with our microscopy software and its construction was amenable to physical modifications. We attached supports ("legs") to the bottom of the OT1 to position the liquid handler above the microscope stage and cut a hole into the baseplate of the OT1 so that the pipette could reach the plate on the microscope stage below (Supplementary Figure 2). We connected the computer directly to the smoothieboard, bypassing the normal OT-1 raspberry pi controller, to directly access the OpenTrons API. Via the OpenTrons API, the FALCOscope system can define pipette configurations, specify the type and location of containers and pipette tips on the liquid-handler, and control robotic movement commands.

The FALCOscope software integrates the liquid handler and microscope APIs by communicating dynamic movement of the imaging plate on the motorized stage relative to the fixed stage of the liquid handler and by coordinating the timing of microscope and liquid handler commands. To track the movement of the imaging plate, the FALCOscope software reads the position of the stage, calculates the change in position since the previous calibration, and then updates the microscope stage positioning in the OpenTrons API. The FALCOscope employs a command queue to coordinate the timing of the microscope and liquid handler commands. The command queue pauses microscope operations when the liquid handler interacts with the imaging plate but otherwise enables the liquid handler to operate independently while the microscope images. The FALCOscope system performs experiments on a 96-well plate one column at a time; the total run length is the number of columns times the time course length (Supplementary Figure 3). This FALCOscope system increases experimental throughput by 8-fold vs. manual addition on individual imaging dishes.

To extract information from the large imaging datasets, we developed automated image analysis software to efficiently quantify cellular responses to stimuli (Supplementary Figure 4). These tools help programmatically access time course image stacks within MATLAB which can be processed using available MATLAB scripts that implement segmentation techniques such as threshold and watershed to distinguish nearby cells from each other[13]. We also incorporated tools to record image segmentation and analysis.

Capturing GPCR-stimulated PKA activity dynamics.

FALCOscope can rapidly acquire detailed, kinetic concentration-response data from live-cell biosensor imaging. As a test, we quantified the Protein Kinase A (PKA) response to the β-adrenergic receptor (βAR) agonist isoproterenol (Iso) in HEK293T cells. HEK293T cells were plated into 96 well glass bottom plates and transfected with AKAR4, a Förster

Resonance Energy Transfer (FRET)-based biosensor that serves as a surrogate substrate of PKA and reports PKA activity via changes in FRET[14]. Using the FALCOscope system, we automated the acquisition of time-course images across wells and the delivery of different Iso concentrations. To quantify the PKA activity response to 14 Iso concentrations at a 1-min time intervals, we collected data in parallel across 8 well columns of the 96 well plate. After 3 min of baseline image acquisition, the OT1 delivered Iso to the wells of a single column using an 8-channel pipette; 15 min later, the OT1 administered a mixture of the AC activator forskolin (Fsk) and the phosphodiesterase (PDE) inhibitor IBMX as a positive control (Figure 2A). We used automated image segmentation to identify individual cells within each image and tracked the cells across the imaging time course to quantify the dynamics at the single-cell level (Figure 2B, Supplementary Figure 5). We then aggregated single-cell responses from several replicate wells and three plate replicates to quantify the temporal response of AKAR4 across the range of Iso concentrations (Figure 2C). Fitting the logistic curve to the single-cell responses at 5.5 min after stimulation revealed that the measured Iso EC50 was 9.47 ± 0.12 nM (Supplementary Figure 6), which is in close agreement with a previously published EC50[15].

The enhanced throughput of the FALCOscope system thus enabled the collection of hundreds to thousands of cells per drug dose. These many single-cell responses improve the accuracy of the average response, enable examination of single cell behaviors and concentration-response variability across different cells, wells, and plates (Supplementary Figure 7).

Probing the functional cAMP response of endogenously expressed GPCRs.

Activated GPCRs that couple to Gs or Gi proteins regulate cAMP production by activation or inhibition, respectively, of AC[16]. Certain assays that assess Gs- and Gi-coupled GPCRs utilize colorimetric or chemiluminescent cAMP readouts but require cell lysis and lack temporal information in live-cells[7,17]. Plate readers can be used to measure live-cell assays using bioluminescent or fluorescent cAMP biosensors but lack single cell resolution[18,19]. In contrast, the FALCOscope system enables high content screens with automated addition of different stimuli and measurement of dynamic cAMP responses in individual living cells.

We profiled cAMP responses of endogenously expressed GPCRs in HEK293 cells to GPCR agonists and antagonists of the Gs-coupled pathway.

We tested the cAMP response to 14 GPCR agonists and antagonists in HEK293 cells transiently transfected with the FRET-based cAMP biosensor Epac-SH188 (H188) to quantitatively measure the Gs-linked GPCR responses[20]. Working in single-column batches across a 96 well plate, we acquired images in 1-min intervals while simultaneously treating each of the 8 wells in a column with a different GPCR agonist or antagonist. The single-cell responses were quantified by automated image segmentation, and the cAMP dynamics were aggregated across the well replicates (Figure 3, Supplementary Figure 8).

The results show that the HEK293 cells exhibit statistically significant Gαs responses to stimulation with adenosine, Iso, epinephrine, PGE1, and PGE2 compared to the vehicle control (Figure 3A). Several GPCRs that can couple to Gi (e.g., Lysophosphatidic acid, oxytocin, angiotensin) did not alter cAMP concentration, presumably due to low basal cAMP levels. The cAMP response to βAR agonists (epinephrine and Iso) and abrogation of the epinephrine- induced cAMP response by co-incubation with the βAR antagonist propranolol indicate endogenous expression of βARs in the HEK293 cells, as demonstrated previously[21–24]. Prior data for adenosine A2B receptors in HEK 293 cells match the observed cAMP response to adenosine[25–28]. The cAMP response to PGE1 and PGE2 indicates endogenous prostaglandin receptors, also previously noted[29,30].

The GPCR induced cAMP dynamics assessed by the FALCOscope enable characterization of Gs-coupled GPCR signaling responses with high sensitivity, detailed temporal information, and single cell resolution. This demonstrates the likely applicability of the FALCOscope for single-cell, dynamic measurements in compound screening or profiling of GPCR activity.

Examination of Gs-linked activation of GPR68.

We next set out to apply the FALCOscope system to characterize GPR68, also known as ovarian cancer G-protein-coupled receptor 1 (OGR1)[31]. GPR68, a member of the class A proton-sensing GPCR family, is active at low pH (6.8 or lower), inactive at high pH (7.8) and couples to both Gs and Gq/11[31,32]. GPR68 is expressed in numerous human cells types including osteoblasts, epithelial cells of the lung, intestine, and renal tubules, airway smooth muscle cells, and various immune cell types; GPR68 expression is increased in several types of cancer, including carcinoma, pancreatic ductal adenocarcinoma, cervical squamous cell carcinoma, and ovarian cancers compared to normal tissues[33]. The G_s response of GPR68 in response to acidic pH has been characterized in model cells lines such as HEK293/HEK293T[31,34–36] and Chinese Hamster Ovary (CHO)[37] cells heterologously expressing GPR68 and in cells that endogenously express GPR68[35,36,38–42]. However, these studies utilized immuno- or luminescence assays and typically measured cAMP at a single time point after 10–40 min preincubation with new pH media and a PDE inhibitor. Leveraging the FALCOscope's live-cell imaging capability and versatility for automated medium exchange, we assessed GPR68-mediated cAMP dynamics in live cells with single cell resolution.

We created a HEK293 cell line stably expressing GPR68 (GPR68OE) and verified GPR68 expression via immunohistochemistry using two different GPR68 antibodies (Supplementary Figure 9). To quantify cAMP dynamics in response to GPR68 activation, we introduced H188 via transient transfection into HEK293 GPR68OE cells and matched HEK293 control cells and used the liquid handler to exchange pH 8.5 imaging media with imaging media at different pH's (Supplementary Figure 10). We confirmed that the automated medium exchange achieves the desired pH by using a pH-dependent fluorescent dye[43] (Supplementary Figure 11). No pH-induced changes occurred in the HEK293 parental line but GPR68OE cell showed cAMP responses at pH's 6.5, 6.8, 7.0, a minor response at pH 7.4, and no response at pH's 8.0 and 8.5, consistent with previous studies[31,34] (Supplementary Figures 10A and 10B).

We next evaluated the effect of ogerin, a positive allosteric modulator (PAM) for GPR68[31]. The FALCOscope system enabled evaluation of real-time cAMP responses to varying pH and ogerin conditions in a single 96 well plate experiment. We treated cells simultaneously with varying pH's and concentrations of ogerin and measured cAMP dynamics in the GPR68 OE and control cells (Figure 4A; Supplementary Figure 12). Ogerin significantly and dose-dependently enhanced cAMP response at pH's greater than pH 6.5 (Supplementary Figure 13). Ogerin (10 μM) increased maximal response at pH's 6.8 and 7.0 to values akin to those at pH 6.5 (Supplementary Figure 14). Consistent with its PAM effect[40], ogerin dose-dependently increased cAMP responses at pH's 7.0 and pH 7.4 (Supplementary Figure 15).

Since the FALCOscope measures cAMP dynamics from individual cell traces, we calculated kinetic parameters to characterize the cAMP dynamic trends, e.g., the time to reach half maximal value ($t_{1/2}$) (Figure 4B; Supplementary Figure 16) and the sustained activity metric at 40 min (SAM40) (Figure 4C; Supplementary Figure 17). Faster responses were observed for acidic (pH 6.8 or 6.5) conditions compared to pH 7.0, in the absence and presence of ogerin (Figure 4B; Supplementary Figure 16). The transient nature of the cAMP responses observed at acidic pH contrasted with the largely sustained responses (from SAM40 analysis) observed at pH 7.0 (Figure 4A, 4C; Supplementary Figure 17). Ogerin also appeared to make cAMP responses more sustained at acidic pH's (Figure 4C). Thus, both the orthosteric and allosteric agonists increase the cAMP response amplitude and affect the kinetic characteristics.

The strong effects of 10 μM ogerin prompted us to perform experiments to test whether ogerin might have effects on cAMP dynamics independent of GPR68 in HEK293 cells that do not express GPR68. HEK293 cells transfected with H188 were treated with ogerin and then activated with several different cAMP/PKA pathway stimulants: by the AC activator Fsk at a low concentration (1 μM) or by endogenously expressed G_s-coupled GPCRs agonists (Iso, PGE2). We measured the total cAMP increase during the 20 min after treatment with Fsk, Iso or PGE2 and then added IBMX to cells pretreated for 20-min with 10 μM ogerin or vehicle (DMSO) control (Supplementary Figure 18). While 10 μM ogerin did not produce a statistically significant effect, 100 μM ogerin increased cAMP responses (Supplementary Figures 18, 19A–C). IBMX treatment after Iso normalized the difference between 100 μM ogerin-pretreated and control cells, implying that higher concentrations of

ogerin might inhibit PDEs (Supplementary Figure 19A–C). A PDE activity assay supported this idea; 100 μM ogerin significantly decreased PDE activity (5'-AMP production) compared to the DMSO vehicle control (Supplementary Figure 19D). Thus, at higher concentrations, ogerin inhibits PDE activity, which likely increases cAMP levels in cells--an important consideration when using ogerin to modulate G_s-coupled GPR68 signaling. This finding is consistent with data showing that three compounds similar to ogerin may have both GPR68 PAM and PDE inhibition activity[31].

CONCLUSION

This work identifies the FALCOscope as an approach to increase throughput of single-cell biosensor imaging. We applied the FALCOscope system to assess GPCR ligands and a proton (pH)-sensing GPCR. For higher throughput screening, commercially available liquid handling combined plate readers can image entire plates and dispense simultaneously to all wells using 96, 384, and 1536 dispensing heads[44]. The FALCOscope has lower throughput compared to those plate readers but measures single cell responses, enabling detection of amplitude and kinetic responses that may be masked in plate reader measurements. Our open-source tool-based system also provides an economical alternative to commercial liquid handling combined plate readers and microscopy-based high content screening systems[45].

Our μManager-based integration approach should be widely applicable to different microscope configurations, enabling this approach for automating and enhancing throughput of live cell biosensor imaging on existing fluorescent microscope set-ups. Adaptation would be needed for the OT2 (OpenTrons), on which the smoothieboard is not directly accessible. This could be done using the OT2 Python-based API and a Jupyter Notebook hosted on the OT2[46]. This system is well-suited for investigating cell signaling kinetics on the timescale of minutes as the FALCOscope can image an entire column within 30 s – 1 min due to the rate-limiting steps of the moving to each well and imaging multiple fluorescent channels per well. We employed this system using a 10X objective; it should be compatible with any air-based objective but not with immersion-media based objectives as the immersion media would be lost during movements across the plate.

Given the modularity of fluorescent biosensors and flexibility of the FALCOscope, various fluorescent biosensors that measure signaling activities and utilize different colors should be compatible with FALCOscope imaging. For example, this approach could be expanded to fluorescent biosensors for GPCR and G-protein activation, calcium dynamics, RhoA activation and ERK activity[47]. Different colors are available for such biosensors, so it should be possible to modify this platform for co-imaging of multiple sensors in individual cells[10,48,49]. The approach could also be applied to imaging subcellularly targeted biosensors to examine spatially compartmentalized signaling[11]. With enhanced throughput, high spatiotemporal resolution and readout of multiple activities, this platform could also be used for high-content screens of compounds that interact with GPCRs and GPCR signaling.

FALCOscope enabled rapid detection of GPR68-mediated cAMP dynamics in response to extracellular pH change and ogerin, a positive allosteric modulator (PAM). From single cell responses, we analyzed cAMP dynamics with three quantitative measures: maximum

response, $t_{1/2}$ of maximum response, and SAM40. We validated findings from previous studies using a luciferase-based cAMP assay, showing that the pH 6.5 induces maximal cAMP response and that 10 μM ogerin left-shifts the concentration-response curve for pH, as expected for a PAM[31]. Our studies reveal a new insight into GPR68-mediated cAMP dynamics: acidic pH stimulation yields faster, more transient cAMP responses. The transient response at acidic pH's is akin to previous data in human airway smooth muscle (HASM) cells that endogenously express GPR68[36].

A possible mechanism for the signaling attenuation at acidic pH's could be pH-induced GPR68 internalization, but whether GPR68 is internalized at acidic pH's is controversial[34,36,50]. Another possible mechanism of transient cAMP dynamics at acidic pH's could be activation of PDE3 and PDE4 by PKA, resulting in enhanced cAMP degradation. We were able to observe this signal attenuation, unlike previous studies[51,52], as we did not pretreat with PDE inhibitors during experiments assessing GPR68 responses. Future studies will explore the regulation of GPR68-mediated cAMP/PKA signaling and functional consequences thereof.

By capturing kinetic information under various conditions, we observed effects of ogerin on cAMP dynamics and signaling amplitude. We found that ogerin has stronger PAM activity in neutral pH environments and sustains cAMP responses at acidic pH's. Other GPR68 PAMs may induce similar effects on cAMP dynamics as observed with ogerin[35,53,54].

Supplementary Material

Refer to Web version on PubMed Central for supplementary material.

ACKNOWLEDGEMENTS

The authors are grateful to R. Wollman (University of California, Los Angeles) for providing automated image acquisition and analysis scripts. C.P. was supported by NIH Grant T32 GM008326 and 1F31 CA257381-01A1. This material is based upon work supported by the National Science Foundation Graduate Research Fellowship Program under Grant No. (DGE-2038238) to A. L. Any opinions, findings, and conclusions or recommendations expressed in this material are those of the author(s) and do not necessarily reflect the views of the National Science Foundation. This work was supported by R35 CA197622, R01 DK073368 and a grant from Fibrolamellar Cancer Foundation (FCF) to J.Z. and by the David Lehr Award from the American Society of Pharmacology and Experimental Therapeutics to P.A.I.

Data and Code Availability.

Data used to generate all graphs are included in the source data file. All other data supporting these findings are available upon reasonable request. The code is available at https://github.com/jinzhanglab-ucsd/FALCOscope.

REFERENCES

1. Sriram K & Insel PA G protein-coupled receptors as targets for approved drugs: How many targets and how many drugs? Mol. Pharmacol 93, 251–258 (2018). [PubMed: 29298813]
2. Insel PA et al. G protein-coupled receptor (GPCR) expression in native cells: 'Novel' endoGPCRs as physiologic regulators and therapeutic targets. Mol. Pharmacol 88, 181–187 (2015). [PubMed: 25737495]

3. Stockert JA & Devi LA Advancements in therapeutically targeting orphan GPCRs. Front. Pharmacol 6, 1–8 (2015). [PubMed: 25805991]
4. Wang W, Qiao Y & Li Z New Insights into Modes of GPCR Activation. Trends Pharmacol. Sci 39, 367–386 (2018). [PubMed: 29395118]
5. Hauser AS, Attwood MM, Rask-Andersen M, Schiöth HB & Gloriam DE Trends in GPCR drug discovery: New agents, targets and indications. Nat. Rev. Drug Discov 16, 829–842 (2017). [PubMed: 29075003]
6. Zhang R & Xie X Tools for GPCR drug discovery. Acta Pharmacol. Sin 33, 372–384 (2012). [PubMed: 22266728]
7. Yasi EA, Kruyer NS & Peralta-Yahya P Advances in G protein-coupled receptor high-throughput screening. Curr. Opin. Biotechnol 64, 210–217 (2020). [PubMed: 32653805]
8. Halls ML & Canals M Genetically Encoded FRET Biosensors to Illuminate Compartmentalised GPCR Signalling. Trends Pharmacol. Sci 39, 148–157 (2018). [PubMed: 29054309]
9. Ni Q, Mehta S & Zhang J Live-cell imaging of cell signaling using genetically encoded fluorescent reporters. FEBS J 285, 203–219 (2018). [PubMed: 28613457]
10. Greenwald EC, Mehta S & Zhang J Genetically encoded fluorescent biosensors illuminate the spatiotemporal regulation of signaling networks. Chem. Rev 118, 11707–11794 (2018). [PubMed: 30550275]
11. Mehta S & Zhang J Biochemical Activity Architectures Visualized-Using Genetically Encoded Fluorescent Biosensors to Map the Spatial Boundaries of Signaling Compartments. Acc. Chem. Res 54, 2409–2420 (2021). [PubMed: 33949851]
12. Edelstein A, Amodaj N, Hoover K, Vale R & Stuurman N Computer control of microscopes using manager. Curr. Protoc. Mol. Biol 1–17 (2010) doi:10.1002/0471142727.mb1420s92.
13. Wollman R & Stuurman N High throughput microscopy: From raw images to discoveries. J. Cell Sci 120, 3715–3722 (2007). [PubMed: 17959627]
14. Depry C, Allen MD & Zhang J Visualization of PKA activity in plasma membrane microdomains. Mol. Biosyst 7, 52–58 (2011). [PubMed: 20838685]
15. Gupta RC, Neumann J, Durant P & Watanabe AM A1-adenosine receptor-mediated inhibition of isoproterenol-stimulated protein phosphorylation in ventricular myocytes: Evidence against a cAMP- dependent effect. Circ. Res 72, 65–74 (1993). [PubMed: 8380264]
16. Denis C, Sauliere A, Galandrin S, Senard J-M & Gales C Probing Heterotrimeric G Protein Activation: Applications to Biased Ligands. Curr. Pharm. Des 18, 128–144 (2012). [PubMed: 22229559]
17. Williams C cAMP detection methods in HTS: Selecting the best from the rest. Nat. Rev. Drug Discov 3, 125–135 (2004). [PubMed: 15040577]
18. Binkowski BF, Fan F & Wood KV Luminescent Biosensors for Real-Time Monitoring of Intracellular cAMP. in Signal Transduction Protocols (eds. Luttrell LM & Ferguson SSG) 263–271 (Humana Press, 2011). doi:10.1007/978-1-61779-160-4_14.
19. Allen MD et al. Reading dynamic kinase activity in living cells for high-throughput screening. ACS Chem. Biol 1, 371–376 (2006). [PubMed: 17163774]
20. Klarenbeek J, Goedhart J, Van Batenburg A, Groenewald D & Jalink K Fourth-generation Epac-based FRET sensors for cAMP feature exceptional brightness, photostability and dynamic range: Characterization of dedicated sensors for FLIM, for ratiometry and with high affinity. PLoS One 10, (2015).
21. Krupinski J, Lehman TC, Frankenfield CD, Zwaagstra JC & Watson PA Molecular diversity in the adenylylcyclase family. Evidence for eight forms of the enzyme and cloning of type VI. J. Biol. Chem 267, 24858–24862 (1992). [PubMed: 1332969]
22. DiPilato LM, Cheng X & Zhang J Fluorescent indicators of cAMP and Epac activation reveal differential dynamics of cAMP signaling within discrete subcellular compartments. Proc. Natl. Acad. Sci. U. S. A 101, 16513–8 (2004). [PubMed: 15545605]
23. Violin JD et al. β2-Adrenergic receptor signaling and desensitization elucidated by quantitative modeling of real time cAMP dynamics. J. Biol. Chem 283, 2949–2961 (2008). [PubMed: 18045878]

24. Tsvetanova NG & von Zastrow M Spatial encoding of cyclic AMP signaling specificity by GPCR endocytosis. Nat. Chem. Biol 10, 1061–1065 (2014). [PubMed: 25362359]
25. Mundell SJ, Loudon RP & Benovic JL Characterization of G protein-coupled receptor regulation in antisense mRNA-expressing cells with reduced arrestin levels. Biochemistry 38, 8723–8732 (1999). [PubMed: 10393547]
26. Mundell SJ, Matharu AL, Kelly E & Benovic JL Arrestin isoforms dictate differential kinetics of A2(B) adenosine receptor trafficking. Biochemistry 39, 12828–12836 (2000). [PubMed: 11041847]
27. Inbe H, Watanabe S, Miyawaki M, Tanabe E & Encinas JA Identification and Characterization of a Cell-Surface Receptor, P2Y15, for AMP and Adenosine. J. Biol. Chem 279, 19790–19799 (2004). [PubMed: 15001573]
28. White CW, Johnstone EKM, See HB & Pfleger KDG NanoBRET ligand binding at a GPCR under endogenous promotion facilitated by CRISPR/Cas9 genome editing. Cell. Signal 54, 27–34 (2019). [PubMed: 30471466]
29. Rich TC et al. Cellular mechanisms underlying prostaglandin-induced transient cAMP signals near the plasma membrane of HEK-293 cells. Am. J. Physiol. - Cell Physiol 292, 319–331 (2007).
30. Zhang JF et al. An ultrasensitive biosensor for high-resolution kinase activity imaging in awake mice. Nat. Chem. Biol 17, 39–46 (2021). [PubMed: 32989297]
31. Huang XP et al. Allosteric ligands for the pharmacologically dark receptors GPR68 and GPR65. Nature 527, 477–483 (2015). [PubMed: 26550826]
32. Ludwig M-G et al. Proton-sensing G-protein-coupled receptors. Nature 425, 93–98 (2003). [PubMed: 12955148]
33. Wiley SZ, Sriram K, Salmerón C & Insel PA GPR68: An emerging drug target in cancer. Int. J. Mol. Sci 20, (2019).
34. Huang YH, Su YS, Chang CJ & Sun WH Heteromerization of G2A and OGR1 enhances proton sensitivity and proton-induced calcium signals. J. Recept. Signal Transduct 36, 633–644 (2016).
35. Pera T et al. Biased signaling of the proton-sensing receptor OGR1 by benzodiazepines. FASEB J 32, 862–874 (2018). [PubMed: 29042451]
36. Nayak AP et al. Regulation of ovarian cancer G protein-coupled receptor-1 expression and signaling. Am. J. Physiol. - Lung Cell. Mol. Physiol 316, L894–L902 (2019). [PubMed: 30724097]
37. Mogi C et al. Sphingosylphosphorylcholine antagonizes proton-sensing ovarian cancer G-protein-coupled receptor 1 (OGR1)-mediated inositol phosphate production and cAMP accumulation. J. Pharmacol. Sci 99, 160–167 (2005). [PubMed: 16210776]
38. Wiley SZ et al. GPR68, a proton-sensing GPCR, mediates interaction of cancer-associated fibroblasts and cancer cells. FASEB J 32, 1170–1183 (2018). [PubMed: 29092903]
39. Tomura H et al. Prostaglandin I2 production and cAMP accumulation in response to acidic extracellular pH through OGR1 in human aortic smooth muscle cells. J. Biol. Chem 280, 34458–34464 (2005). [PubMed: 16087674]
40. Liu JP et al. Ovarian cancer G protein-coupled receptor 1-dependent and -independent vascular actions to acidic pH in human aortic smooth muscle cells. Am. J. Physiol. - Hear. Circ. Physiol 299, (2010).
41. Saxena H et al. The GPCR OGR1 (GPR68) mediates diverse signalling and contraction of airway smooth muscle in response to small reductions in extracellular pH. Br. J. Pharmacol 166, 981–990 (2012). [PubMed: 22145625]
42. Wang J, Sun Y, Tomura H & Okajima F Ovarian cancer G-protein-coupled receptor 1 induces the expression of the pain mediator prostaglandin E2 in response to an acidic extracellular environment in human osteoblast-like cells. Int. J. Biochem. Cell Biol 44, 1937–1941 (2012). [PubMed: 22835475]
43. Doughty MJ PH dependent spectral properties of sodium fluorescein ophthalmic solutions revisited. Ophthalmic Physiol. Opt 30, 167–174 (2010). [PubMed: 20444121]
44. Vetter I et al. High-Throughput Fluorescence Assays for Ion Channels and GPCRs. in Advances in Experimental Medicine and Biology vol. 1131 27–72 (2020). [PubMed: 31646506]

45. Li L, Zhou Q, Voss TC, Quick KL & LaBarbera DV High-throughput imaging: Focusing in on drug discovery in 3D. Methods 96, 97–102 (2016). [PubMed: 26608110]

46. Ouyang W et al. An Open-Source Modular Framework for Automated Pipetting and Imaging Applications. Adv. Biol 6, (2022).

47. Clister T, Mehta S & Zhang J Single-cell analysis of G-protein signal transduction. J. Biol. Chem 290, 6681–6688 (2015). [PubMed: 25605723]

48. Mehta S et al. Single-fluorophore biosensors for sensitive and multiplexed detection of signalling activities. Nat. Cell Biol 20, 1215–1225 (2018). [PubMed: 30250062]

49. Mo GCH, Posner C, Rodriguez EA, Sun T & Zhang J A rationally enhanced red fluorescent protein expands the utility of FRET biosensors. Nat. Commun 11, 1–9 (2020). [PubMed: 31911652]

50. Tan M, Yamaguchi S, Nakamura M & Nagamune T Real-time monitoring of pH-dependent intracellular trafficking of ovarian cancer G protein-coupled receptor 1 in living leukocytes. J. Biosci. Bioeng 126, 363–370 (2018). [PubMed: 29655915]

51. Terrin A et al. PGE1 stimulation of HEK293 cells generates multiple contiguous domains with different [cAMP]: Role of compartmentalized phosphodiesterases. J. Cell Biol 175, 441–451 (2006). [PubMed: 17088426]

52. Matthiesen K & Nielsen J Cyclic AMP control measured in two compartments in HEK293 cells: Phosphodiesterase K M is more important than phosphodiesterase localization. PLoS One 6, (2011).

53. Yu X et al. Design, Synthesis, and Characterization of Ogerin-Based Positive Allosteric Modulators for G Protein-Coupled Receptor 68 (GPR68). J. Med. Chem 62, 7557–7574 (2019). [PubMed: 31298539]

54. Foster SR et al. Discovery of Human Signaling Systems: Pairing Peptides to G Protein-Coupled Receptors. Cell 179, 895–908.e21 (2019). [PubMed: 31675498]

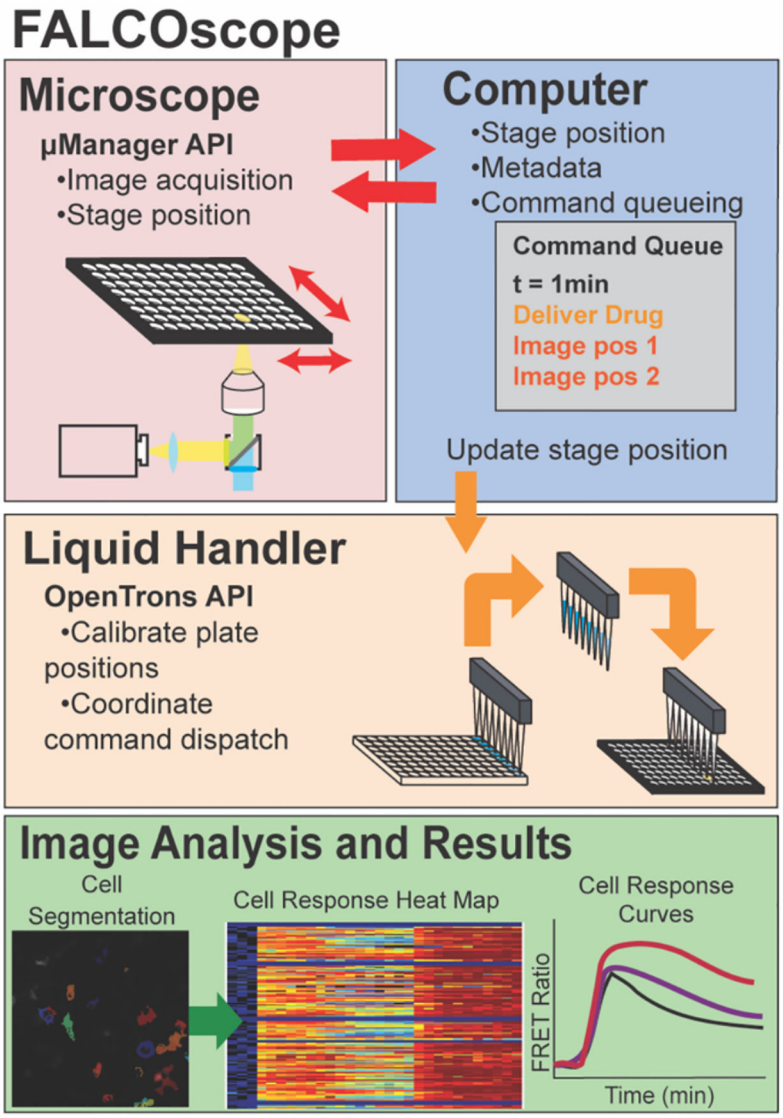

Figure 1.

A schematic of how the FALCOscope coordinates between the microscope and the liquid handler using the µManager application program interface (API), the OpenTrons API from the OT-1 and an imaging queue system. Custom MATLAB scripts segment cells from the fluorescent images and output a table of measured single cell responses over time along with associated metadata that can be plotted in various ways.

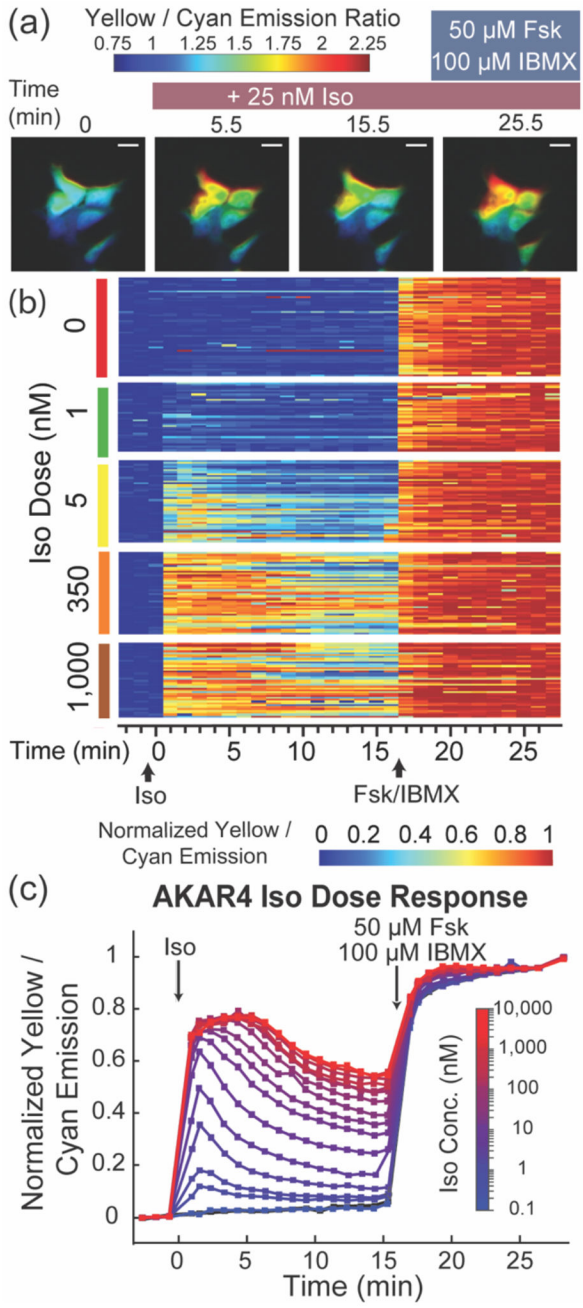

Figure 2.

Protein Kinase A (PKA) response measured by AKAR4 to the βAR agonist isoproterenol (Iso) in HEK293T cells. (A) Representative pseudo color images of time course imaging. Scale bars equal 20 μm. (B) A heat map of single-cell temporal responses of AKAR4 to Iso stimulation for representative Iso doses. Cell numbers listed in Table S1. (C) The average biosensor responses over time for each Iso concentration normalized to baseline and max values.

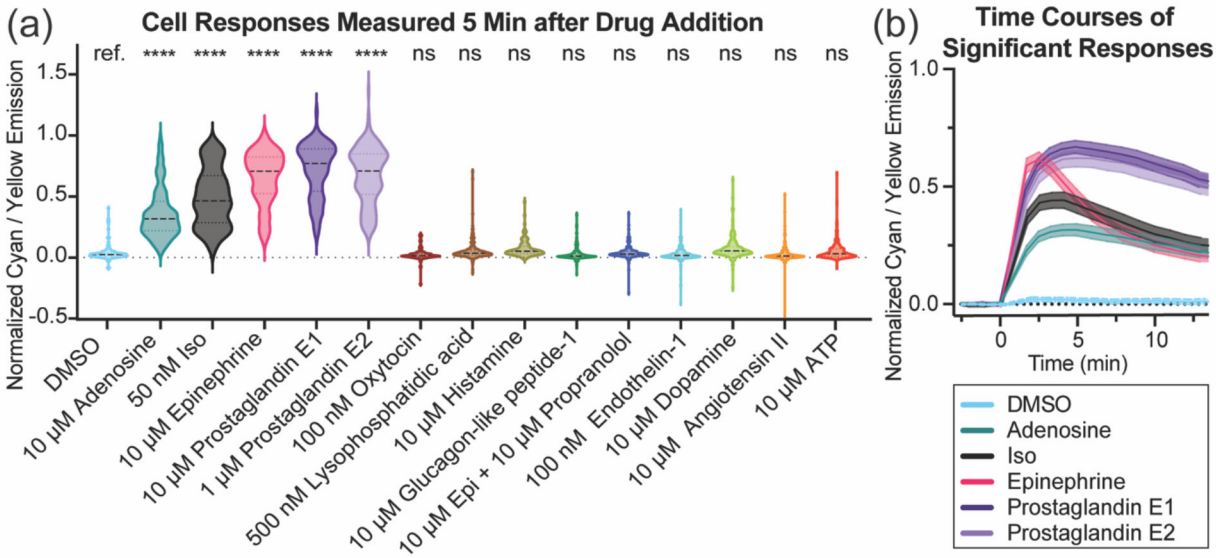

Figure 3.

Measuring the cAMP response of endogenously expressed Gs- and Gi-coupled GPCRs using agonists and antagonists and the CY-FRET cAMP biosensor Epac-SH188. (A) Quantification of individual responses 4–5 min after GPCR agonist or antagonist addition compared with vehicle (DMSO) control. ns =not statistically significant, **** $p < 0.0001$; one-way ANOVA with Dunnett's multiple comparisons test. Cell numbers and exact statistical parameters listed in Tables S2 and S3. (B) The time-course of statistically significant cAMP responses compared to the DMSO.

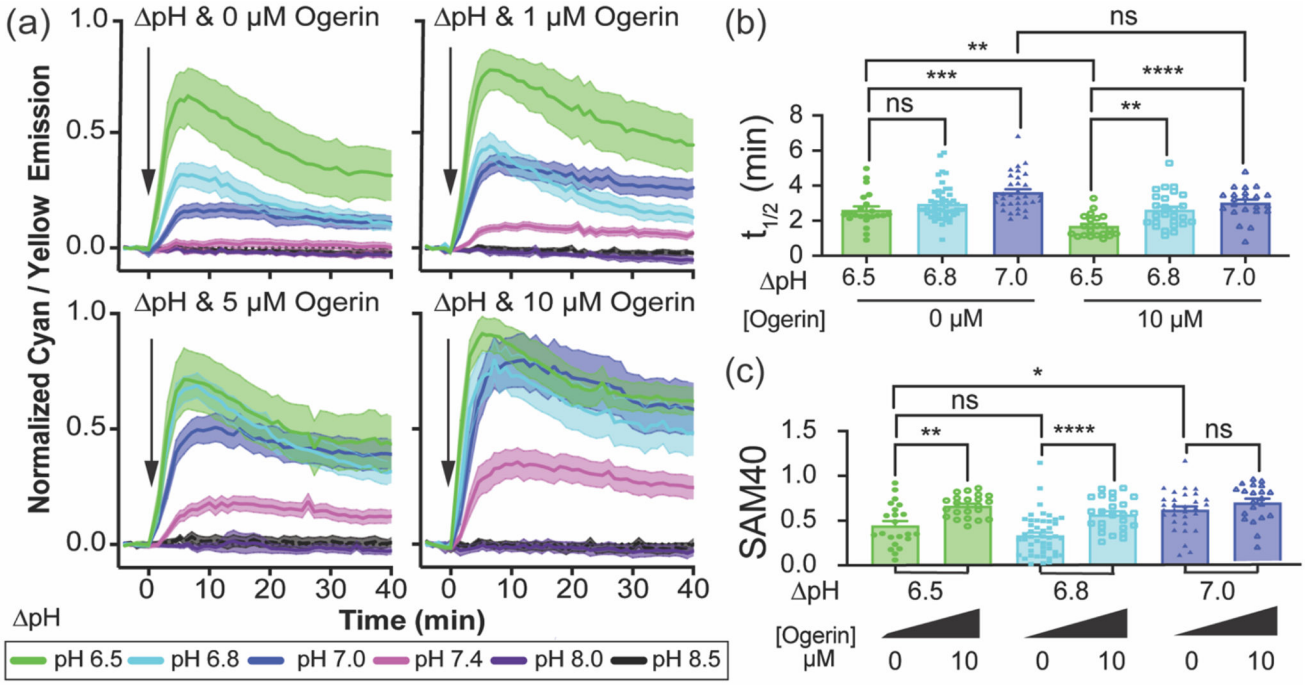

Figure 4.

G_s-linked activation in HEK293 cells stably expressing GPR68 (GPR68OE) transiently transfected with Epac-S^{H188}. Cells were incubated in pH 8.5 HBSS and then with concentrations of ogerin at different pH's. (A) Time-courses of average cAMP response with 95% CI error bars for each pH for treatments compiled from single cell responses from two independent experiments. Cell number for each condition is listed in Table S4. (B) Time to half maximal activation ($t_{1/2}$) calculated from the single cell traces displayed with +/− SEM error bars. (C) Sustained Activity Metric at 40 min (SAM40) calculated from the single cell traces displayed with +/− SEM error bars. Ns = not statistically significant, * $p < 0.05$, ** $p < 0.01$, *** $p < 0.001$, **** $p < 0.0001$; one-way ANOVA with Dunnett's multiple comparisons test. Exact statistical parameters in Tables S5 and S6.